East European Journal of Physics. 3. 501-508 (2023)
DOI:10.26565/2312-4334-2023-3-57 ISSN 2312-4334

EFFECT OF GeO_2 DOPANTS IN FBG SENSOR PERFORMANCE FOR TEMPERATURE AND STRAIN[†]

Wasmaa A. Jabbar[a†], Ayser Hemed[a]*, Mayyadah Fadhala[b‡], Ismaeel Al-Baidhany[a§]
[a]*Department of Physics, College of Education, Mustansiriyah University, Baghdad, Ipak*
[b]*Alsalam Distinguished Students Secondary School, 2nd Karkh directorate of education, Baghdad, Ipak*
**Corresponding author e-mail: ayser.hemed@uomustansiriyah.edu.iq, †E-mail: wasmaajabbar@uomustansiriyah.edu.iq*
‡*E-mail: mayads539@gmail.com;* §*E-mail: ismaeel_2000@uomustansiriyah.edu*
Received May 7, 2023; revised June 19, 2023; accepted June 19, 2023

In this simulation study, the response of fiber Bragg grating (FBG) sensors is investigated and optimized. Uniform and nonuniform FBG spectra with new component are suggested by fine selection with (COMSUL program) and compared theoretically under the effect of several external strain values (0.005, 0.006, 0.007, 0.008, 0.009 and 0.01). These two types operation have been examined by the Optisystem programmer. The measured sensitivity was based on VCSEL laser source with operation wavelengths of 1650, 1600, and 1550 nm via non-uniform and uniform configuration. The achieved sensitivity was found to have different values; 5.7, 2.6, and 1.77, while the highest observed sensitivity value is recorded at a wavelength of 1550 nm. Accordingly, this wavelength was chosen to advance the study. Temperatures of 20, 30, 40, 50, and 60 degrees Celsius were applied. Measured sensitivity between them varied, and satisfied the following functions: sine, Gauss, and Boltzmann indicating altering in sensor responses.
Key words: *FBG sensor; Bragg wavelength; Elastic-optical coefficient; Thermo-optic effect; Strain-optic effect; Sellmeier formula*
PACS: 42.81.-i: 42.81. Pa

INTRODUCTION

Due to their sensitivity, dependability, low intrusiveness, galvanic insulation, and potential for quasi-distributed remote measurements, optical fiber sensors based on fiber Bragg grating (FBG) technology are used in a variety of fields, including civil engineering and aviation [1]. In addition, monitoring strain [2], vibration [3] and temperature [4].

Furthermore, the FBG sensor itself has recently been continuously enriched by research due to its applications in optical communications [5], such as smart frequency filtering [5], [6], [7], dynamical encrypting with chaotic communications [8], [9], [10], [11].

FBGs are extensively utilized in optical sensing and can compete with traditional electrical strain gauges to determine various parameters, such as temperatures, strain, refractive index, pressure, gas, etc. Furthermore, FBG sensors have been widely recognized for their features such as erosion resistance, resistance to electro-magnetic (EMI) and radio frequency interference, and ability to operate in harsh environments where traditional sensors cannot [12].

Since more than few decades, FBG sensors have meets a lot of attention in the field of structural health monitoring [13] [14]. Earlier application of these types of sensors is load screening and characterizing absolute strain and temperature variations, either individually [15] or at the same time [16]. Changes in average strain and temperature would primarily cause a change in the location of the resonance wavelength of the FBG output due to their linear wavelength shift response [17]. The whole reflection spectra of the sensor output signal are, however, affected by the strain (or even temperature) field.

The shape and wavelength shift of the reflection spectra were measured and studied by simulation in this study to investigate the impacts of strain and temperature changes dispersed along the length of FBG sensors. Under these two circumstances, shifts were examined using various FBG architectures.

More benefits than that mentioned above are recorded to FBG based sensors, such as small size, light weight, high resolution, multiplexing capability, and immunity to electromagnetic fields. They have been used in biological diagnosing and structural health monitoring [18]. Due to its uniquely intelligent physical properties, such as its innately huge multiplexing capacities, remote sensing, resistance to electromagnetic fields, and safety, the uniform FBG sensor has been extensively used in sensing applications [12]. The UFBG sensor are also used in dynamical spectral filters invented inside fibers [19].

THEORETICAL CONCEPTS

The FBG transmits all wavelengths of light while reflecting some due to the periodic (or aperiodic) disruption in the refractive index of its core, known as gratings. The Bragg wavelength, at which there is the most reflection, can be determined by applying the following equation [15]:

$$\lambda_{Br.} = 2n_{eff}\,\Lambda \tag{1}$$

[†] ***Cite as***: W.A. Jabbar, A. Hemed, M. Fadhala, I. Al-Baidhany, East Eur. J. Phys. 3, 501 (2023), https://doi.org/10.26565/2312-4334-2023-3-57
© W.A. Jabbar, A. Hemed, M. Fadhala, I. Al-Baidhany, 2023

where n_{eff} is the effective refractive index of the grating and Λ is the grating period.

Strain has two distinct impacts on a Bragg grating. First, the grating's Bragg wavelength will shift as a result of the alteration in the physical distance between succeeding index modulations. Second, a change in refractive index brought on by the strain-optic effect will result in a shift in the Bragg wavelength. For a specific change in strain, the change in a Bragg grating's center wavelength is given by [20]:

$$\Delta\lambda_{Br.} = 2\left[\Lambda\frac{\partial n_{eff}}{\partial l} + n_{eff}\frac{\partial\Lambda}{\partial l}\right]\Delta l \tag{2}$$

where l is the effective length.

An optical fiber's strain effect is depicted in equation (2). This is consistent with a shift in grating spacing and the strain-optic-induced shift in refractive index. [20]. Under the condition of a uniform strain along the optical fiber axis and no temperature changes, the wavelength shift is related to the strain via the elastic-optical coefficient $\mathcal{P}e$ [20]:

$$\Delta\lambda_{Br.} = \lambda_{Br.}(1-\mathcal{P}e)\varepsilon \tag{3}$$

Equation (3) points out that the resulted shift in Bragg peak wavelength is linearly proportional to the applied strain. In the sensing theory of FBG, the strain value should be expressed as;

$$\varepsilon = \frac{\Delta\lambda_{Br.}}{\lambda_B(1-\mathcal{P}e)} \tag{4}$$

where ε is the strain along the lengthwise direction of the fiber and $\mathcal{P}e$ is an effective strain optic constant, which is defined as [1]:

$$\mathcal{P}e = \frac{n_{eff}^2}{2[\mathcal{P}_{12}-\upsilon(\mathcal{P}_{11}+\mathcal{P}_{12})]} \tag{5}$$

Such that $\mathcal{P}_{11}$ and $\mathcal{P}_{12}$ are strain-optic tensor two components, and υ is the ratio of Poisson. For a typical Germano-Silicate optical fiber, p_{11} = 0:113, p_{12} = 0:252, = 0:16, and n_{eff} = 1.45, giving [21] $\mathcal{P}_{12}$ = 0:213.

SIMULATION PART

Selection for refractive index concentration by COMSOL Software

By applying the last values in eq. (5), we got the value of $\mathcal{P}e$ (effective strain optic constant). The calculated value of $\mathcal{P}e$ was then used in eq. (3) for the specific wavelengths 1550, 1600, and 1650 nm for each strain value (0.005, 0.006, 0.007, 0.008, 0.009). Finally, we got the values of shift in wavelength for each value of strain, and for each wavelength, as shown in tables 1, 2, and 3.

Via COMSOL simulation, numerical Finite Element Method (FEM) has been used for the modal analysis of an optical fiber. This fiber is designed to investigate the effect of doping concentration of both core and clad silica glass to the application as a sensor. The variation of the effective refractive index has a significant impact on the sensitivity of such fiber sensors. The influence of doping silica optical fiber with Ge in a different concentration. Also doping concentration effect on effective refractive index and optical intensity has been. The refractive index has been calculated for the doped silica fiber with Ge samples by Sellmeier formula:

$$n(\lambda) = \left[1 + \sum_{i=1}^{M}\frac{A_i\lambda^2}{\lambda^2-\lambda_i^2}\right]^{1/2} \tag{6}$$

For dopants GeO_2, n is the optical index at light wavelength λ and λ_i is a constant such that λ_1, λ_2, λ_3 and A_1, A_2, A_3 are called Sellmeier coefficients to be determined by the fitting process. This means measuring the refractive index of the medium at least for six different wavelengths. In this study, identical last coefficients are calculated, to approximate the dispersion curve.

Measurement of temperature by FBGs

Measurement of temperature, a crucial parameter in various sectors of industry, can be done with the help of FBGs. As reported by Ref. [22], both low and high temperatures can be measured using FBGs with equal accuracy. However, practically measurement of high temperature with FBGs poses some additional challenges compared to others. In this section, we shall discuss the FBG-based temperature sensors subjected to no variation in other physical parameters of the FBG.

Analytical formulation for temperature measurement

The Bragg wavelength (λ_B) of an FBG can be expressed as [23] [17]:

$$\lambda_{Br.}(T) = 2n_{eff}(T)\Lambda(T) \tag{7}$$

Hence, a small change in operating temperature T will result a change in the peak wavelength which can be represented as [17]:

$$\delta\lambda_{Br.} = \frac{d\lambda_{Br.}}{dT}\delta T = 2\left(\Lambda\frac{dn_{eff}}{dT} + n_{eff}\frac{d\Lambda}{dT}\right)\delta T = \lambda_{Br.}\left(\frac{1}{n_{eff}}\frac{dn_{eff}}{dT} + \frac{1}{\Lambda}\frac{d\Lambda}{dT}\right)\delta T \quad (8)$$

So, the change in the temperature can be retrieved directly from $\Delta\lambda$ [24]:

$$\lambda_{Br.} = \lambda_{Br.}(\alpha_{n,T} + \alpha_{\Lambda,T})\delta T = \lambda_{Br.}(\xi + \beta_T)\delta T \simeq \lambda_{Br.}\xi\delta T \quad (9)$$

Therefore, it is possible to control the mechanical and thermal expansion coefficients by changing the cross-section characteristics. It is important that the packaging allows for a limited range of temperature variation. At high temperatures approaching the melting point of the packaging material, the packaging starts to distort whereby the Young's modulus begins to change and thus the thermal expansion coefficient will no longer exist. The work has been done on achieving the highest sensor sensitivity [25].

Simulation set-up design for FBG operation by Optisystem software

As given in Figure (1), a VCSEL laser source with 1550 nm operation wavelength is selected to submit the optical signal. This source is followed with a directional coupler with equivalent splitting ratio. One of these two new paths is considered as a reference path, while the remaining path represents the tested path. Both reference and tested paths include a distinct FBG, i.e., the refence one contains a standard Uniform FBG sensor, the remaining path contains a laboratory Nonuniform FBG sensor. Two types of observation tools are connected, which are, Optical spectrum analyzers (OSA) and optical time domain, virtual oscilloscopes (OTV) both for track the development for passed signals during the experiment conditions variations.

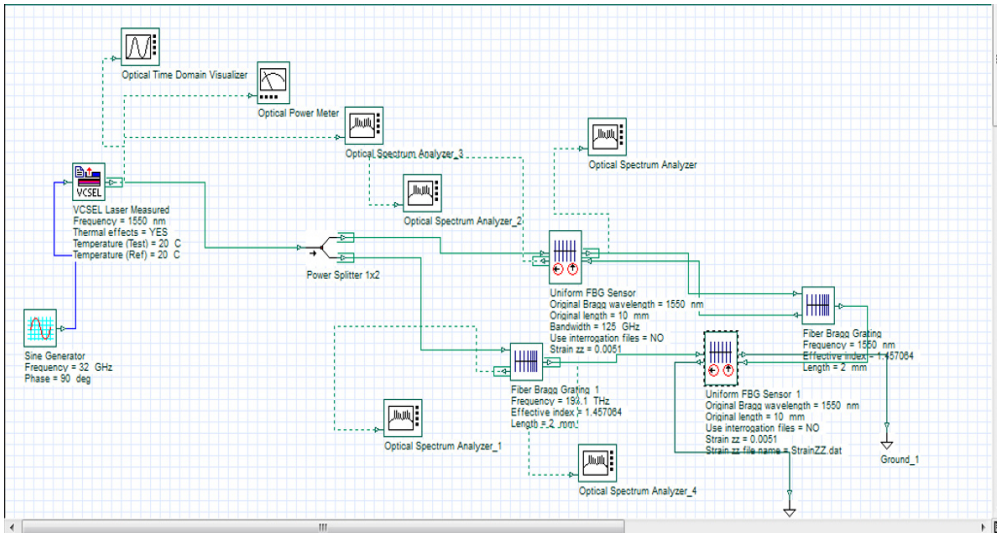

Figure 1. Simulation set-up for the investigated design.

RESULTS AND DISCUSSION

The two types of suggested FBGs have identical constant Bragg wavelengths before the application of the external environmental effect. Original effective length in the software is changed by values 10, 20, 30 all in mm units. The selected effective refractive index for both FBGs is n_{eff}=1.45, with length of 2mm.

Measurements for UFBG

Effect of strain on sensing wavelength shift

Three Bragg wavelengths ($\lambda_{Br.}$) for investigated FBG sensors were tested, these wavelengths are: 1550, 1600 and 1650 nm. Calculations for the deflected wavelength shift is carried out manually and individually for each wavelength by using of eq. (5). Where the measured shifts are resulted from the virtually applied strain. The latter effect selected values are: (0.005, 0.006, 0.007, 0.008, 0.009, 0.01) µm, as shown in tables 1.

Table 1. Theoretical computed wavelengths shift for tested UFBGs sensors λ_{Br}

Initial wavelength $\lambda_{Br.}$ (nm)	Strain Experienced by FBG	Wavelength shift (nm)
1550	0.005	6.1987755
	0.006	7.4385306
	0.007	8.6782857
	0.008	9.9180408
	0.009	11.1577959
	0.01	12.397551

Initial wavelength $\lambda_{Br.}$ (nm)	Strain Experienced by FBG	Wavelength shift (nm)
1600	0.005	6.398736
	0.006	7.6784832
	0.007	8.9582304
	0.008	10.2379776
	0.009	11.5177248
	0.01	12.797472
1650	0.005	6.5986965
	0.006	7.9184358
	0.007	9.2381751
	0.008	10.5579144
	0.009	11.8776537
	0.01	13.197393

Results for the first run measurements are given in the following table (2) and resulted relations are shown in the next Figure (2).

Table 2. Calculated sensitivity for indicated UFBGs sensors $\lambda_{Br.}$

Bragg wavelength value $\lambda_{Br.}$ (nm)	Sensitivity (pm/^{0}c)
1550	5.7
1600	2.6
1650	1.77

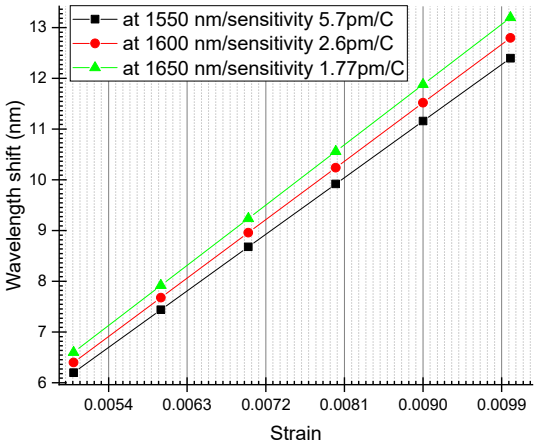

Figure 2. Resulted for strain – wavelength relations to the tested UFBGs sensor.

According to calculated results for sensitivity given in table (4), the selection is located at the maximum value, which is 5.7 pm/^{0}c which corresponds to 1550 nm. A strain–wavelength A strain–wavelength relation, with an effective wavelength of 1.45, is plotted in Figure (2), and the resultant shape is followed by a linear fitting. Accordingly, from Figure (2), part A, 1550 nm, the maximum measured sensitivity value is (5.7) corresponding to wavelength (1550) with a sensitivity of 5.7 pm/^{0}c, while in the same figure, part B, 1600nm, the maximum measured sensitivity value is (2.6) corresponding to wavelength (1600) with a sensitivity of 2.6 pm/^{0}c, finally in part C, 1650nm, the maximum measured sensitivity value is (1.77) corresponding to wavelength (1650) with a sensitivity of 1.77 pm/^{0}c.

Effect of temperature on sensing wavelength shift

In current study, the stabilization of type I gratings complies with telecommunication requirements, thus the selected temperature range is 20-60 ^{o}C, this is based on range given in Ref. [26]. In the following Figure (2), deflected measured Bragg wavelength shift is plotted against sensitivity for seven temperature values, all ranging from 20 to 60 ^{o}C. The FBGs parameters are as follows: effective refractive index of 1.45, length 2mm, wavelength of 1550nm. The temperature and wavelength are changing as given in Figure 3(A), for an original length of 10 mm.

Temp. values range from 20.3331 to 60.067^{o}C, while wavelengths range from 1.549976 nm to 1.54995272 nm. While in the same figure, part (B), for the original length of 20mm, T values range from 20.0353 to 60.0672135^{o}C, but wavelength range from 1.54997726 to 1.54997686 nm. In part (C) from the same figure, for an original length of 30mm, the temperature ranges from 19.9327865, to 59.9646844 ^{o}C, but the wavelength is now ranging from 1.54991417 to 1.54995338 nm. In part (D), after doping, T values range from 20.0353156 to 59.8735475 ^{o}C, but wavelengths range from 1.54984538 to 1.54984468 nm.

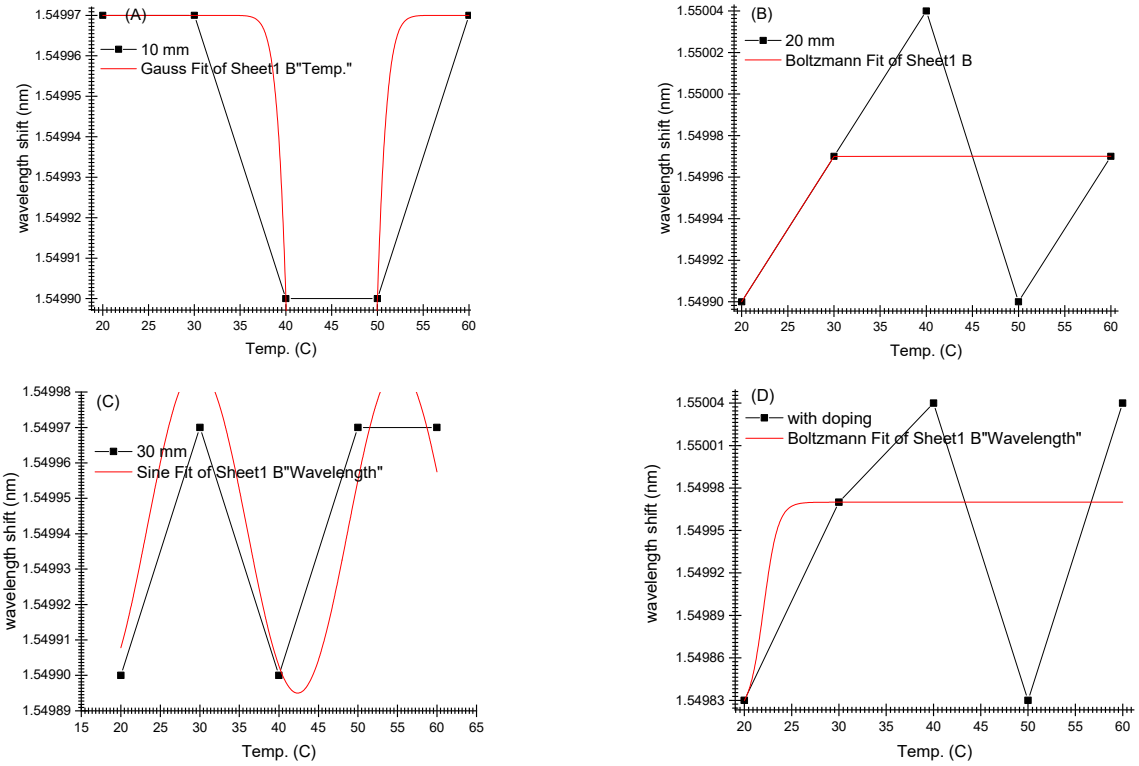

Figure 3. Results for temperature – shifted wavelengths with changed sensor temp.
(A) L=10mm, (B) L=20mm, (C) L=30mm (D) after dopping

For the same previous set-up, the transmitted power spectrum is observed separately for each FBG applied temperature. Results are given in the following Figure (4), with which transmitted power behavior fluctuates from sine function to Gauss. The temperature and wavelength are changed as the following form: in part (A) for the original length 10mm from 20.0353156 to 60.1583504 ºC, but the transmitted power (TR) was changed from TR=8.96362864 to 9.02625248 ºC. In part (B), for the original length of 20mm, T is changed from 20.0353156 to T=60.0672135 ºC, but the transmitted power is changed from TR=8.49448061 to 8.5161336 ºC. Finally, in part (C), T is changed from 20.4226475 to 60.0672135 ºC, while the transmitted power is changed from TR = 7.4483448 to 7.45740164 ºC.

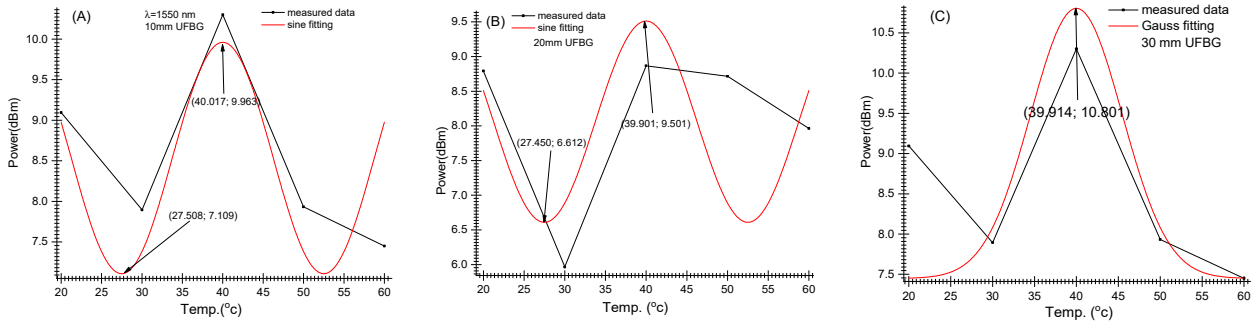

Figure 4. Results for power- temperature variation in UFBG with lengths; 10 mm (B) 20 mm and, (C) 30 mm

Measurements of NUFBG

Effect of temperature on sensing wavelength shift

In this section, insertion of a signal of 1550 nm wavelength into the input of NUFBG has been carried out where the FBG has specific active lengths; 10, 20, and 30mm and a constant effective refractive index of 1.45 with variable applied temperature. Results observed from the deflection side give different responses, as shown in Figure (5) and its entire subfigures A, B, C and D based on equation (6). As shown in part (A), the FBG active length was 10mm from T=20.1264 ºC to T=59.9646844ºC, but the wavelength ranged from 1.54989965 nm to 1.54996984 nm, as shown in part (A). The FBG active length was 20 mm from T = 20.1264525ºC to T = 59.9646844ºC in part (B), but the wavelength ranged from 1.54992244 nm to 1.54984271 nm in part C. Finally, in part D, after doping, the effective refractive index is constant at 1.46 with variable applied temperature gives different responses as deflected wavelengths from T=19.8416496 ºC to T=5 8735ºC. The wavelengths are 1.54996967 nm to 1.54984357 nm.

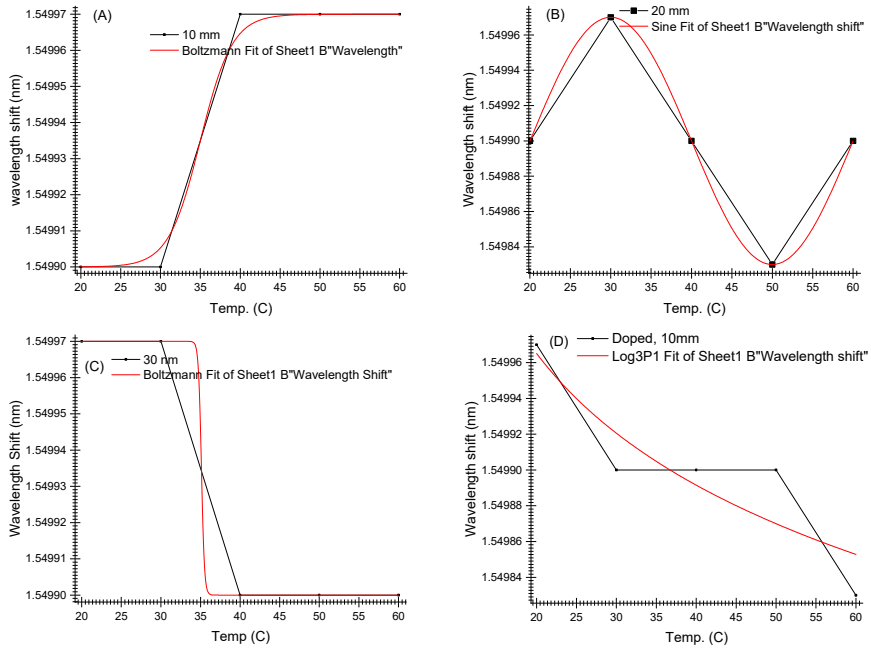

Figure 5. Results for shifted wavelength – applied temperature for a NUFBG with lengths (L) in mm. (A)10, (B) 20, (C) 30 and (D) 10, after doping

These results indicate the existence of three types of behavior functions followed by the NUFBG under the influence of applied temperature. In the dopant case, these two functions are Boltzmann and sine in additional logarithm. Under the influence of variable applied temperature, we expect to meet a different response than that measured by UFBG. Previous results shown in Figure (3), indicates the response with only a sine function.

Effect of temperature on sensing power

In the case of measuring power instead of wavelength, the results for NUFBG response indicate variant Gauss functions depending on active sensor wavelength, shown in Figure (6). In comparison to last section results, in which the response obeys varied functions. For the same previous setup, transmitted spectrum power is measured for each applied temperature. Observed values for temperature and wavelength is shown inside part (A) from that figure, for the original length of 10 mm. While in part (B) and (C), another observed value is diagnosed. With comparisons by Ref. [27], the current combination is 1.5 times larger sensitivity than it.

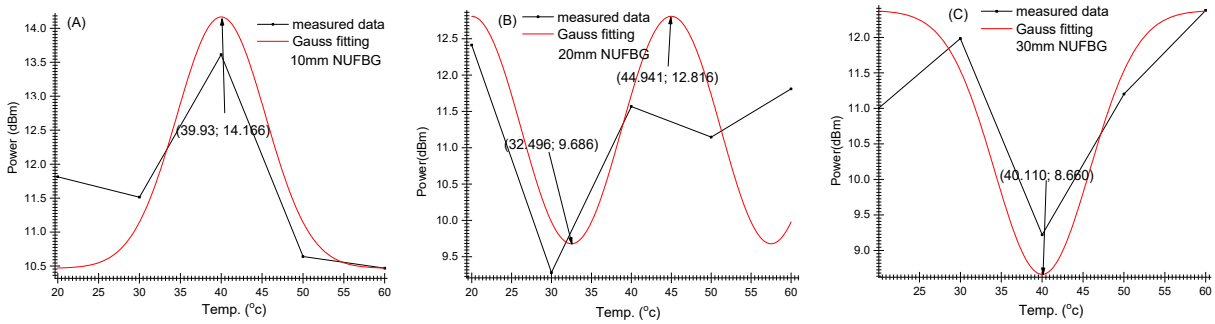

Figure 6. Results for power-temperature relations for different NUFBGs lengths (L) in mm. (A) 10, (B) 20 and (C) 30.

Uniform and nonuniform FBG Sensor design of (L=10mm) active length with Bragg wave length 1550 nm tested under temperatures (20- 60 °C) with step 10 degree.

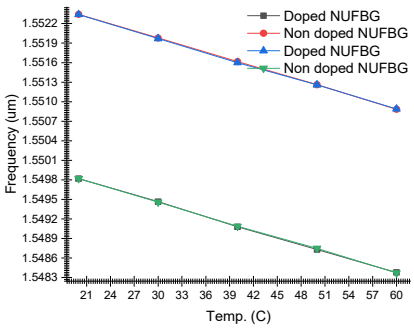

Figure 7. Measured values of wavelengths and intensity for uniform FBG before and after doping

Where the values plotted in figure (7) are drawn from radio frequency spectra for all tested values which is given in figure (8). In which the frequency shift is easy to observe versus the changed parameter in comparisons with multi regions FBG that experimentally investigated by Ref. [6].

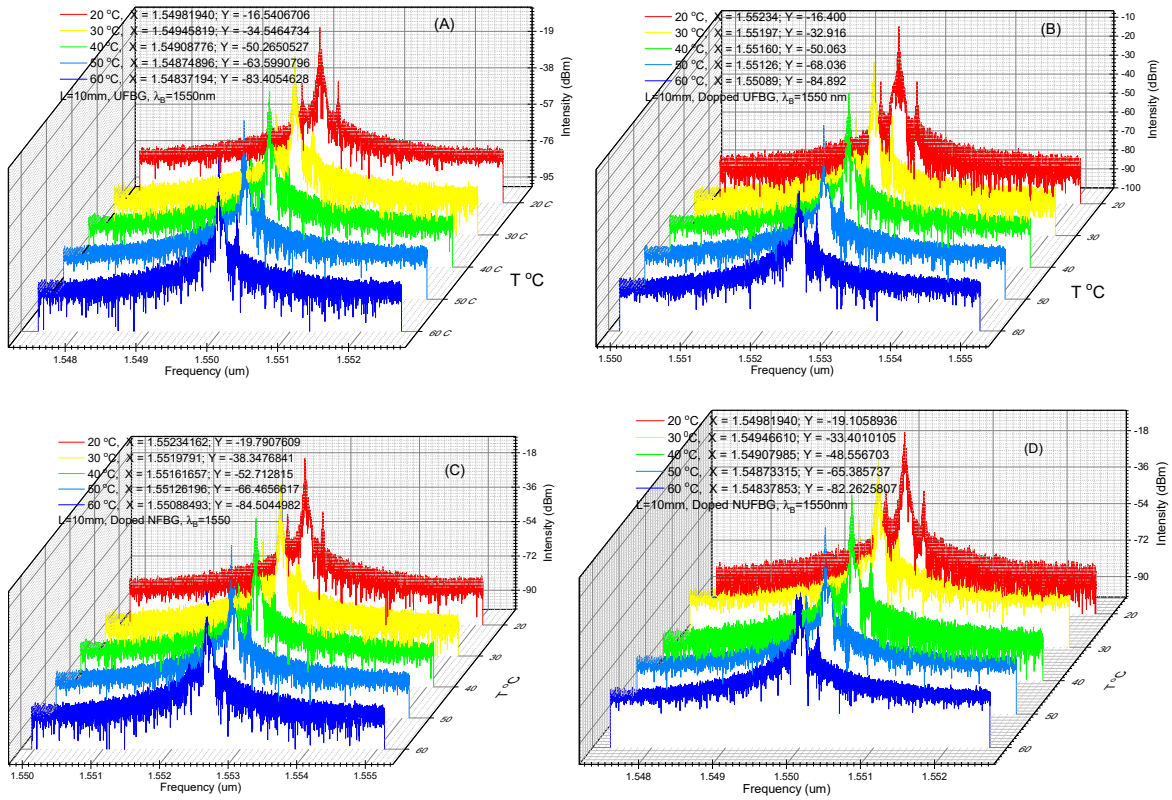

Figure 8. Results for reflected spectra shift for: (A) Non-doped UFBG, (B) Doped UFBG, (C) Non-doped NUFBG, and (D) Doped NUFBG.

CONCLUSIONS

Constructing FBG combination improves the sensing properties for the FBG sensor. Uniform and non-uniform FBGs plays the role of precise filter to the temperature and strain fluctuations. The sensitivity becomes high with introducing impurities of GeO_2 dopants. Results for shifted wavelength – applied temperature for a NUFBG shows variations from Poltizman to Log. Functions, while the same measurements for power-temperature relations for lengths shows behaviors fluctuated within one function which is a Gauss function.

Acknowledgement: Authors for the study would like to thank Mustansiriyah University (www.uomustansiriyah.edu.iq) Baghdad, Iraq for support in the present work.

ORCID

Ayser Hemed, https://orcid.org/0000-0003-0319-1650; **Wasmaa A. Jabbar**, https://orcid.org/0000-0003-3966-9468
Ismaeel Al-Baidhany, https://orcid.org/0000-0001-5273-9921

REFERENCES

[1] B.A. Tahir, M.A. Saeed, A. Ahmed, S.M.Z. Iqbal, R. Ahmed, M.G.B. Ashiq, H.Y. Abdullah, and R.A. Rahman, "Effect of Sensor Gauge Length on Strain Sensitivity of a Fiber Bragg Grating System," Chinese Journal of Physics, **49**(5), 1035-1045 (2011).
[2] J. Zhou, Z. C. Orcid, P. Zhao, and A. Tang, "Efficient Sensor Placement Optimization for Shape Deformation Sensing of Antenna Structures with Fiber Bragg Grating Strain Sensors," Sensors, **18**(8), 2481 (2018). https://doi.org/10.3390/s18082481
[3] F. Xiao, G.S. Chen, and J.L. Hulsey, "Monitoring Bridge Dynamic Responses Using Fiber Bragg Grating Tiltmeters," Sensors (Basel), **17**(10), 2390 (2017). https://doi.org/10.3390/s17102390
[4] Y. Liu, and J. Zhang, "Model Study of the Influence of Ambient Temperature and Installation Types on Surface Temperature Measurement by Using a Fiber Bragg Grating Sensor," Sensors, **16**(7), 975 (2016). https://doi.org/10.3390/s16070975
[5] M. Fdhala, and S.M. Khorsheed, "Characterization of Uniform FBG sensor Operation for Signal Filtering Application," European Journal of Advances in Engineering and Technology, **7**(2), 1-6 (2020).
[6] A.A. Hemed, M.M. Fdhala, and S.M. Khorsheed, "Modified superstructure fiber Bragg grating for a filter application," Kuwait J. Sci. **49**(1), 1-18 (2022). https://doi.org/10.48129/kjs.v49i1.12487
[7] S.M. Khorsheed, A.A. Hemed, and M.M. Fdhala, "Investigation of Performance for a Two Regions Superstructure Fiber Bragg Grating," World Scientific News, **137**, 42-57 (2019). http://www.worldscientificnews.com/wp-content/uploads/2019/09/WSN-137-2019-42-57.pdf

[8] Z.R. Ghayib, and A.A. Hemed, "Simulating chaotic dynamics with variable polarisation of VCSEL twin lasers using FBG as a dynamic sensor," Pramana – J. Phys. **96**, 86 (2022). https://doi.org/10.1007/s12043-022-02305-2
[9] Z.R. Ghayib, and A.A. Hemed, "Smart control for the chaotic dynamics using two regions uniform fiber Bragg grating," Optoelectronics and advanced materials-Rapid communications, **16**(7-8), 307-318 (2022).
[10] A.A. Hemed and Z.R. Gaiab, "Chaotic Dynamics for VCSEL Subjected to Time Delayed and Filtered Injection Using FBG Array Sensor," in: *2022 International Conference on Computer Science and Software Engineering (CSASE)*, Duhok, Iraq, 2022. pp. 194-200, https://doi.org/10.1109/CSASE51777.2022.9759612
[11] A.A. Hemed, Z.R. Ghayib and H.G. Rashid, "Controlling a chaotic anti-synchronized oscillator by a phase interplayed optical injected seed with an FBG sensor," in: *2nd International Conference on Physics and Applied Sciences (ICPAS 2021) 2nd International Conference on Physics and Applied Sciences (ICPAS 2021), College of Education, Mustansiriyah University*, Baghdad, Iraq, (2021). https://doi.org/10.1088/1742-6596/1963/1/012063
[12] Q.-b. Wang, H.-t.Z.Y. Qiu, J.-a. Chen, Y.-y. Wang, and Z.-m. Fan, "Analysis of strain transfer of six-layer surface-bonded fiber Bragg gratings," Applied Optics, **51**(8), 4129-4138 (2012). http://dx.doi.org/10.3390/app8071171
[13] I.A. Naseef, A.I. Mahmood, A.A. Jabor, M.M. Azzawi, S.A. Kadhim, N.F. Muhammed, and W.A. Jabbar, "Characterization study of modified cladding optical fibre sensor for low radiation dosimeters," AIP Conference Proceedings, **2290**, (2020). https://doi.org/10.1063/5.0027535
[14] W.A. Jabbar, N.F. Muhammad, S.A. Kadhim, A.H. Dagher, A.I. Mahmood, and I.A. Naseef, "Investigation the doping influence on the characteristics of optical fiber for radiation dosimeter applications," Materials Today: Proceedings, **20**, 524-530 (2020). https://doi.org/10.1016/j.matpr.2019.09.181
[15] Y.-J. Rao, "In-fibre Bragg grating sensors," Measurement Science and Technology, **8**(4), 355 (1997). https://doi.org/10.1088/0957-0233/8/4/002
[16] Y. Mizutani, and R.M. Groves, "Multi-Functional Measurement Using a Single FBG Sensor," Experimental Mechanics, **51**(9), 1489-1498 (2011). https://doi.org/10.1007/s11340-011-9467-2
[17] R. Kashyap, *Fiber Bragg Gratings 2nd Edition*, (Academic Press, Montréal, 2009).
[18] K. Grattan, and T. Sun, "Fiber optic sensor technology: an overview," Sensors and Actuators A: Physical, **82**(1-3), 40-61 (2000). https://doi.org/10.1016/S0924-4247(99)00368-4
[19] A.S Mansour, and F.M. Abdulhussein, "Dual Measurements of Pressure andTemperature With Fiber Bragg Grating Sensor," Al-Khwarizmi Engineering Journal, **11**(2), 86-91 (2015). https://www.iasj.net/iasj/pdf/eef5012601618008
[20] J. Frieden, J. Cugnoni, J. Botsis, and T. Gmür, "Low energy impact damage monitoring of composites using dynamic strain signals from FBG sensors – Part II: Damage identification," Composite Structures, **94**(2), 593-600 (2012). https://doi.org/10.1016/j.compstruct.2011.08.025
[21] A. Onoufriou, K. Kalli and G. E. Kohnke, "Fiber Bragg Gratings: Fundamentals and Applications in Telecommunications and Sensing," Physics Today, **53**(5), 61-62 (2000). https://doi.org/10.1063/1.883086
[22] C.V.N. Bhaskar, S. Pal, and P.K. Pattnaik, "Recent advancements in fiber Bragg gratings based temperature and strain measurement," Results in Optics, **5**, 100130 (2021). https://doi.org/10.1016/j.rio.2021.100130
[23] K.O. Hill, and G. Meltz, "Fiber Bragg grating technology fundamentals and overview," Journal of Lightwave Technology, **15**(8), 1263-1276 (1997). https://doi.org/10.1109/50.618320
[24] E.S.D.L. Filho, M.D. Baiad, M. Gagné, and R. Kashyap, "Fiber Bragg gratings for low-temperature measurement," Optics Express, **22**(22), 27681-27694 (2014). https://doi.org/10.1364/OE.22.027681
[25] M.R. Mokhtar, T. Sun, and K.T.V. Grattan, "Bragg Grating Packages With Nonuniform Dimensions for Strain and Temperature Sensing," IEEE Sensors Journal, **12**(1), 139-144 (2012). https://doi.org/10.1109/JSEN.2011.2134845
[26] M. Cavillon, M. Lancry, B. Poumellec, Y. Wang, J. Canning, K. Cook, T. Hawkins, P. Dragic, and J. Ballato, "Overview of high temperature fibre Bragg gratings and potential improvement using highly doped aluminosilicate glass optical fibres," Journal of Physics: Photonics, **1**(4), 042001 (2019). https://doi.org/10.1088/2515-7647/ab382f
[27] J. Lai, J. Qiu, H. Fan, Q. Zhang, Z. Hu, J. Wang, and J. Chen, "Fiber Bragg Grating Sensors-Based In Situ Monitoring and Safety Assessment of Loess Tunnel," Journal of Sensors, **2016**, 8658290 (2016). https://doi.org/10.1155/2016/8658290

ВПЛИВ ДОПАНТІВ GeO_2 НА ХАРАКТЕРИСТИКИ ДАТЧИКА FBG ДЛЯ ТЕМПЕРАТУРИ І ДЕФОРМАЦІЇ

Васма А. Джаббар[a], Айсер Хемед[a], Майяда Фадхала[b], Ісмаїл Аль-Байдхані[a]
[a]Кафедра фізики, педагогічний коледж, університет Мустансірія, Багдад, Ірак
[b]Середня школа видатних учнів Алсалам, 2-й Карх директорат освіти, Багдад, Ірак

У цьому моделювальному дослідженні досліджується та оптимізується відгук датчиків волоконної бреггівської решітки (FBG). Рівномірні та неоднорідні спектри FBG з новим компонентом пропонуються шляхом тонкого відбору за допомогою (програма COMSUL) і теоретично порівнюються під впливом кількох значень зовнішньої деформації (0,005, 0,006, 0,007, 0,008, 0,009 і 0,01). Ці два типи роботи були перевірені програмістом Optisystem. Виміряна чутливість була заснована на лазерному джерелі VCSEL з робочими довжинами хвиль 1650, 1600 і 1550 нм через нерівномірну та однорідну конфігурацію. Виявлено, що досягнута чутливість має різні значення; 5,7, 2,6 та 1,77, а найбільше значення чутливості спостерігалося на довжині хвилі 1550 нм. Відповідно, ця довжина хвилі була обрана для просування дослідження. Застосовувалися температури 20, 30, 40, 50 і 60 градусів Цельсія. Виміряна чутливість між ними змінювалася та задовольняла такі функції: синус, Гаусс і Больцман, що вказує на зміну відповідей датчика.

Ключові слова: *датчик FBG; довжина хвилі Брегга; пружно-оптичний коефіцієнт; термооптичний ефект; тензооптичний ефект, формула Зелмайєра*